GTP as an enzymatic synchronizer

Chen-Jun Guo, Xian Zhou and Ji-Long Liu*

School of Life Science and Technology, ShanghaiTech University, Shanghai 201210, China

*Correspondence. Ji-Long Liu. Email: liujl3@shanghaitech.edu.cn

Keywords

- CTP synthase; GTP; glutamine-dependent amidotransferase; amidoligase; synchronizer

Abstract

Synchronizer is the key component of modern automobile gearbox, which coordinates the deceleration and acceleration of two groups of gears. In industry, synchronizer is composed of several components with fine structure. Here, we show that guanosine triphosphate (GTP) has the property of enzyme synchronizer. Through cryo-electron microscopy (cryo-EM) and 3D variability analysis, we obtain the full spectrum conformation of CTP synthase at near atomic resolution. In the catalytic process of CTP synthase, we find that GTP synchronizes the reaction of two independent domains, namely, glutamine-dependent aminotransferase (GAT) domain and amidoligase (AL) domain. The wing structure acts as a striker, and then stimulates the intermediate ammonia to complete the catalytic cycle through the internal gas channel. Different from being degraded to regulate tubulins or G-proteins, GTP acts as an enzymatic synchronizer to coordinate the reactions catalyzed by the two independent domains of CTP synthase.

Main

Life needs metabolism. Metabolism is vital and complex. In a cell, the basic unit of life, there are many metabolic pathways that need to coordinate with each other. Therefore, it is very important to study the regulation of metabolic enzymes. A classic example of understanding metabolic regulation is CTP synthase (CTPS), which has been studied for nearly 70 years, including comprehensive studies in biochemistry, kinetics and structural biology (Anderson, 1983; Aronow and Ullman, 1987; Bakovic et al., 2007; Bearne et al., 2001; Chakraborty and Hurlbert, 1961; De Clercq, 1993; Endrizzi et al., 2004, 2005; Goto et al., 2004; Ingerson-Mahar et al., 2010; Jiménez and O'Sullivan, 1994; Kizaki et al., 1982, 1985; Kizaki et al., 1981; Levitzki and Koshland, 1969, 1971, 1972a, b; Levitzki et al., 1971; Lewis and Villafranca, 1989; Liu, 2010; Long and Pardee, 1967; McPartland and Weinfeld, 1979; Noree et al., 2010; O'Sullivan et al., 1991; Ozier-Kalogeropoulos et al., 1994; Ozier-Kalogeropoulos et al., 1991; Robertson and Villafranca, 1993; Savage and Weinfeld, 1970; Thomas et al., 1988; van Kuilenburg et al., 1998; van Kuilenburg et al., 2000; von der Saal et al., 1985; Weinfeld et al., 1978; Weng and Zalkin, 1987; Willemoës, 2003, 2004; Willemoës and Sigurskjold, 2002; Williams et al., 1978; Wu and Liu, 2022; Yang et al., 1996; Yang and Carman, 1995). CTPS, which consists of two domains, the glutamine-dependent aminotransferase (GAT) domain and the amidoligase (AL) domain, catalyzes the last

step of de novo CTP synthesis (Bearne et al., 2022). CTP is not only as one of the few basic units of RNA and DNA, but also the precursor of membrane phospholipid biosynthesis, protein glycosylation and innate antiviral immunity.

For the study of CTPS, we have learned many basic principles of enzyme regulation (Bearne et al., 2022; Bearne et al., 2001; Iyengar and Bearne, 2003; Lunn and Bearne, 2004; Lunn et al., 2008; MacDonnell et al., 2004; McCluskey and Bearne, 2018a, b; Roy et al., 2010; Simard et al., 2003; Steeves and Bearne, 2011). Recently, we have obtained the conformation of high-resolution CTPS, especially the GTP binding state for the first time (Zhou et al., 2021). However, how precisely GTP plays a role in CTPS regulation remains elusive. The structural knowledge we obtained through crystallography in the past is still the snapshots during the enzymatic reaction. How to understand the whole reaction process through high-resolution structural biology is still an unsolved scientific problem.

In order to understand the dynamic regulation of enzymatic reaction, we take advantage of the ‘resolution revolution’ of cryo-EM (Cao et al., 2013; Cheng, 2015, 2018; Liao et al., 2013). We incubate ligand mixture with the enzyme and then start the reaction. By this means, we can obtain most, if not all, conformations in the full spectrum of the enzymatic reaction.

Through further classification and reconstruction, we can theoretically obtain the whole process of dynamic regulation of enzyme reaction cycle.

We add various ligands to *Drosophila melanogaster* CTPS (dmCTPS). During the reaction, we obtain a large number of high-resolution conformations of CTPS. To our surprise, we find that the reactions catalyzed by GAT and AL domains are highly synchronized. GTP is the key molecule to achieve the synchronization of these two domains. Therefore, our work reveals that GTP plays a vital role as a synchronizer, although it is not a substrate and does not participate in any reaction in CTPS.

Based on our structural data, we propose the concept that GTP as an enzymatic synchronizer. This concept provides a new perspective for CTPS regulation. Our study also raises a series of interesting questions. For example, does GTP also play the role of synchronizer in other enzymes? Is there a GTP like synchronizer in other enzymes? The exploration of these questions will help us gain new insights into the regulation of metabolism.

ACP-inhibited CTPS structure at near atomic resolution

Using analogues of protein ligands to inhibit protein reaction and capture specific states for morphological studies is a common experimental

strategy in structural biology. In our previous study, we successfully inhibited the reaction of GAT domain by 6-diazo-5-oxo-l-norleucine (DON) in CTPS without affecting the AL domain. This time, we chose AMP-PCP (hereinafter referred to as ACP) to replace ATP to inhibit AL domain.(Figure S1) By using Cryo-EM, we solved the tetramer and oligomer structure at 3.2 Å resolution of dmCTPS+Sub (ACP) (Figure1A and Figure S2 ,3).

In the newly obtained ACP binding structure (hereinafter referred to as ACP state), CTPS tetramers rotate to form a filamentous structure. The contact interface between tetramers is similar to the filamentous structure of DON binding state and CTP inhibition state previously found in *Drosophila melanogaster*, which is still formed by pi-pi interaction of h355 α- Helix and surrounding amino acids (Figure 1B).

Compared with the previous DON binding and CTP inhibition states, the tetramer conformation based on the average electron density map has changed greatly. On the basis that the AL domain is in a similar position, in the tetramer of ACP state, the GAT domain has a counterclockwise inward rotation compared with CTP state and a clockwise outward rotation compared with DON state (Figure S4A). ACP, UTP, Mg and GLN were successfully captured in the structure (Figure 1C-F).

Consistent with the theoretical prediction, ACP binds to the original ATP binding position (Figure 1D), and the binding of UTP and Mg is also shown (Figure 1E). Compared with ADP previously captured in the reaction state, their binding modes are generally the same, but slightly different (Figure S4B) The position and binding pocket of α, β phosphoric acid remain the same, but because ACP cannot be hydrolyzed, its γ and β phosphate remain bonded. At a higher contour level, there is a good density separation between γ-phosphate and UTP head (Figure S4C), which indicates that the non-cleaved ACP successfully limits the first step reaction of AL domain.

GTP stimulates GAT reaction

Although AL domain is inhibited by ACP, GAT domain still has substrate GLN and can react (Figure 1F). We found that in the average density of ACP state, the B-factor of synthase domain in the middle of the tetramer is generally between 20 and 50, relatively stable. In contrast, the GAT domain and B-factor around the tetramer are generally between 70 and 120, more active (Figure 2A). Through further dynamic analysis of the data, we successfully captured the dynamic changes of GAT domain from open to close states, which is consistent with the feature of B factor. The two AL domains remain in the same position, and the GAT domain has a rotation of 3.2° around the axis, which also indicates that the GAT domain is in reaction(Figure 2B).

By displaying the calculation results in the simple mode, we obtained a series of structures. One of the components shows the transition of GAT domain from open state to close state.

At frame 0, the GAT domain is open. F373, which is responsible for stabilizing GLN and GTP binding, shows the characteristics of instability (Figure 2C). At the same time, little density is in GLN binding pocket. This indicates that the GAT domain is in the apo state. As the frame moves forward, the loop$^{50\text{-}58}$ where the gate H55 is located, referred to as the “arch” from here on, gradually approaches and the GLN binding pocket appears density.

At frame 6, the density similar to the substrate appears in the GLN binding pocket. At the same time, F373 is also stable, and the arch continues to change towards the closed state (Figure 2D). This confirms the role of F373 in stabilizing Gln binding, and also implies the progress of GAT reaction.

At frame 14, compared with the open state, C399 has additional vacancy density around it, and its side chain also shows different binding modes, which indicates that the substrate and enzyme have formed intermediate products (Figure 2E). We found an additional density on the closed state

side, which connects F373 to the arch and is located at the GTP binding site found in the DON state (Figure 2F). Through the movie (Sup Movie1), the emergence of GTP is quite clear.

The interaction between GTP ribose and arch was stabilized, and arch was pushed to AL domain through the contraction of GAT domain. R376, which plays a key role in GTP binding, has also been stabilized. After the ribose part is bound, the pi-pi interaction between GTP pyrimidine head and F373 provides additional support for the GAT pocket, and its density is further filled. (Figure 2F; Sup Movie1) According to the study of GAT family, the stabilization of GAT reaction pocket by GTP will promote the reaction at the same time. This confirms the conclusion of previous biochemical experiments and provides a structural basis for the promoting effect of GTP on GAT reaction.

Capture of GTP binding in reaction state

Next, we prepared samples containing all substrates including GLN, UTP, ATP, the coenzyme $MgCl_2$ and the allosteric regulator GTP. During sample preparation, we incubated the enzyme with UTP, ATP, GTP and $MgCl_2$. After hydrophilizing the grid, we added excess GLN to start the whole reaction, then quickly dropped the sample solution on the grid and immediately put it into liquid ethane by Vitrobot to prepare Cryo EM

samples. Finally, 300 kV Titan Krios electron microscope was used to data collection. After similar processing to ACP state, the tetramer structure at 3.2 Å resolution of dmCTPS + sub (mix) state were obtained (Figure 3A; Figure S5,6).

In the captured structure, CTPS takes tetramer as the basic unit, and there is the formation of filamentous structure, and its contact interface is consistent with the filamentous structure previously observed (Figure 3B), indicating that the formation of filamentous structure can still be maintained in the reaction. In the average electron density, GLN, UTP and ATP are successfully captured, and their conformations are very similar to the average structure of ACP(Figure 3C,D,E; Figure S7). However, under this condition, we captured a stable density in the GTP binding site in the average map (Figure 3F).

Compared with GTP previously captured in DON state, the conformation of GTP is similar to that of DON state, which exists in a folded manner, a part of magnesium ion above triphosphate stabilizes the negative group, and the binding site is still around L11 and the arch(Figure 3G).

However, the wing(Loop$^{440\text{-}448}$), which plays an important role in GTP regulating CTPS reaction, is not stabilized in the MIX state, but presents an

open form. After lacking the embedding and support of L444 and surroundings, GTP has a shift against the arch, accompanied by the movement of Loop105-109 of another protomer (Figure 3G). These phenomena may be related to the incomplete closure of CTPS (Figure S7).

R481 plays key role in GTP binding

R481 is located in a highly conserved RHRHR motif. It is known that the main chain of this motif is involved in the GLN binding, but the function of their side chains is still lacking.

In mix state, the interaction between R481 and GTP is captured. Comparing to ACP state, without GTP binding, the side chain of R481 exists stably in a form deviating from GTP. After GTP binding, it rotates and interacts with GTP (Figure 3H). Compared with DON state, the way of R481 interacting with GTP has changed, the electrostatic interaction between them has changed from O6 of GTP and NE of arginine to O6 of GTP and NH_2 of arginine (Figure 3G). These phenomena indicate that the recognition and stable combination of GTP by CTPS is closely related to R481.

The arch couples CTPS reaction with GTP

The arch is the major part of NH_3 tunnel and plays key role in the CTPS

reaction. However, we still know little on the way it functions. By using similar strategy with ACP state, the dynamic analysis obtained in mix state provides valuable evidence for us to answer these questions. (Figure 4A; Sup Movie2)

The CTPS structure shown in frame 0 is the most open state in the whole series. We observed that the AL domain combines UTP and ATP but does not start the catalytic reaction. ATP remains intact at this time (Figure 4B). E145 and D70, which are responsible for catalyzing the first step reaction of AL domain, have not yet interacted with ATP (Figure 4B).

Similarly, the GAT domain is in the apo state; the wing is completely open and very flexible; F373 presents an unstable state similar to that observed in CTP; and there is no excess density in the catalytic pocket (Figure 4B). At the same time, the gate H55 is well separated from the density of substrate (Figure 4B). There is no stable density at the GTP binding pocket, and L4 also shows an open pattern, far away from the tetramer center. Consistent with the observation in ACP state, the R376 side chain of apo state is flexible and has no stable density (Figure 4B).

These phenomena show that CTPS is in the stage where the first step reaction of AL domain has not yet occurred, GAT domain does not bind

ligands, and GTP does not form a stable binding with CTPS.

From frame 0 to frame 5, CTPS shows a shrinking trend as a whole, and the GAT domain is close to the AL domain (Figure 4C). During this period, L1 and Helix1, which are responsible for binding and stabilizing ATP, drive ATP to make a small displacement in the AL domain, which makes ATP β Phosphoric acid is close to E145 and D70, which are responsible for catalysis, providing a further basis for the reaction (Figure 4D). At the same time, helix of K228 and loop of P191, which are responsible for combining and stabilizing UTP in the adjacent protomer, push UTP to ATP, and the whole AL domain begins to close (Figure 4D).

With the movement of UTP, the arch begins to move to the AL domain (Figure 4D). The GAT domain began to contract and F373 showed a closed trend, which was very similar to the GLN binding observed in the ACP state (Figure 4D).

These phenomena indicate that in the process of AL closure, the GAT domain is also combining substrates and moving closer to the AL domain.

From frame 6 to 10, CTPS continues to shrink and the GAT domain continues to move to the AL domain (Figure 4E). D70 in the AL domain,

which is responsible for catalyzing ATP cleavage, began to contact ATP (Figure 4F). At the same time, in the GAT domain, RHRHR motif of β19 moves to F373. With the filling of density, GLN binding site enters the closed state (Figure 4F). In frame 6, the ribose of GTP seems to be further stabilized by the arch. As it continues to approach the AL domain and the GAT domain is closed and stabilized, the triphosphate density of GTP is stabilized in frame 6. This is very similar to the GTP binding pattern previously observed in ACP state (Figure 4F).

Combined with the previous conclusions in the ACP inhibited state, these phenomena show that the stable binding of GTP depends on the progress of AL domain and GAT domain reaction, and the arch plays key role in identifying and coordinating the reaction with GTP.

R481 paves the way for the interaction between wing and GTP

From frame 10 to frame 14, after GTP binding, CTPS continues to change to the closed state, and the reaction in the two domains continues (Figure 5A). In the AL domain, the increasing density shows that the interaction between D70 and ATP is gradually enhanced (Figure 5B). The interaction of H55 and UTP has also become stronger, which drives the arch to move further to the AL domain (Figure 5B). The movement of the arch also drives the GTP combined with it to approach the AL domain (Figure 5B). Other

parts interacting with GTP, L4 and L11, have displacement close to the AL domain to varying degrees. The GAT domain continues to catalyze the reaction and approaches AL domain driven by GTP. We note that during the movement of GAT, At frame 14, the disordered R481 becomes stable and interacts with GTP purine oxygen (Figure 5B).

From frame 14 to 19, under the action of GTP, the GAT domain of CTPS continues to shrink and close to the AL domain which is also in the process of contraction (Figure 5C). Finally, the whole CTPS changes to the closed state similar to that captured in the previous DON state. The binding of GTP was further stabilized, R481 continued to move to GTP, and the action with purine head became similar to the mode in DON state, which was more stable (Figure 5D). The movement of R481 drives the β19 and β20 around it towards GTP. Through the interaction between the β sheet skeletons, the edge portion of the GAT domain is pulled and further retracted (Figure 5D). With this movement, at frame 19, we observed that the wing, which was flexible in the reaction, gradually stabilized, showing a conformation similar to that in the DON state (Figure 5D).

Previously, we confirmed that the wing plays an important role in GTP mediated CTPS reaction. Interesting, results of dynamic analysis show that the wing is flexible until R481 interacting with the preliminary stable GTP

(Figure 5B, D), which means that the necessity of the wing for reaction is not reflected in the combination of GTP, but in the role after the R481 stabilizes the GTP.

GTP controls transient ammonia tunnel formation

NH_3 released in GAT domain acts as a nucleophile in the AL domain reaction. To avoid the formation of NH_4^+, CTPS uses a transient internal gas tunnel to transport NH_3. Through biochemical experiments, people found that GTP plays an important role in the ammonia tunnel. In previous study, we revealed that GTP was a component of the ammonia tunnel. Through the newly obtained structure and dynamic analysis, we found that in the process of CTPS reaction, GTP controls the formation of transient ammonia tunnel.

Without GTP binding, in the ACP state model, GAT domain is in reaction and AL domain is inhibited, we found that even though the AL domain and GAT domain combined their respective substrates, ammonia channels did not form at this time (Figure 6A, B). Firstly, the empty GTP binding site generates a large cavity for the tunnel. And the size of this cavity reaches 3.0 Å, which means that the ammonia tunnel has not completed the connection with GAT active sites at this time (Figure 6B, C). Secondly, without the interaction of GTP, the gate H55 and surrounding amino acids

restricts the diameter of ammonia tunnel outlet less than 2Å, prohibiting the passage of ammonia to AL active site (Figure 6B, D; Figure S8A).

When the GTP is preliminary binding, in the mix state, GAT and AL domain are both in reaction, the ammonia tunnel completes the connection of the two active centers (Figure 6E, F). Firstly, under the action of GTP, the catalytic triad completes the connection with the tunnel, and the diameter of the previous hole was limited to less than 2.4 Å, which avoids the leakage of ammonia (Figure 6F, G). Secondly, with the interaction of GTP, the conformation of H55 and surrounding ammonia acids is changed, so that the pore diameter at the outlet reaches more than 3.0Å, allowing the passage of ammonia (Figure 6F, H; Figure S8B). At the same time, the closure of the AL domain also connects the ammonia channel with the active site, making it possible for ammonia to contact the 4Pi-UTP generated by AL domain.

When the GTP is tightly binding with the interaction of wing and L4, in the DON state, the GAT domain is about to complete the reaction and AL domain completes the reaction, the ammonia tunnel is further stabilized (Figure S9A, B). By interaction with wing and L4, GTP is further embedded and moved to GAT pocket (Figure S9C). These conformational changes not only strengthen the connection between the two domains but also

stimulate the release of ammonia. With the generation of 4pi-UTP, the conformation of H55 is changed, the pore diameter of the outlet is modified to about 2.6Å, stabilizing the ammonia to contact the 4Pi-UTP (Figure S9D).

Discussion

In this study, we mixed various ligands in conditions, and then obtained the conformations of different states of CTPS with near atomic resolution by cryo-EM. Through a series of conformational analysis, we can turn some snapshots we usually see into a dynamic process. In this dynamic process, we find that the two domains of CTPS, although they catalyze independent reactions, these reactions are highly synchronized. Through further detailed analysis, we discover that GTP plays a crucial role in the synchronization of the catalytic reactions of the two domains.

As an example of the complexity of protein regulation, CTPS is famous for its regulation by transient internal gas tunnels, multi ligand interactions, different proteomes, different oligomers and post-translational modifications (Bearne et al., 2001; Endrizzi et al., 2004; Goto et al., 2004; Ingerson-Mahar et al., 2010; Levitzki and Koshland, 1971, 1972a; Levitzki et al., 1971; Liu, 2010; Noree et al., 2010; Willemoës, 2003; Williams et al., 1978; Yang et al., 1996). CTPS is composed of two domains: GAT and AL domain (Bearne et al., 2022). Previous studies have shown that the two domains

are very independent in function and structure, while the synthesis of CTP depends on the alternating reaction of the two domains (Bearne et al., 2022). In order to achieve the required efficiency of biological enzymes and the effectiveness of resource use, the coordination and synchronization of the two domains are extremely important. Biochemical experiments and X-ray crystallography emphasize the separation of different domains, and examine the problem from the perspective of solid state. Through 3D variability analysis technology, we bring a dynamic perspective to this problem.

Our study provides a model for the catalytic mechanism of CTPS assisted by GTP with GLN as substrate (Figure 7). At the beginning, with the emergence of UTP and ATP of substrate, CTPS monomer or dimer began to assemble to form tetramer with catalytic activity, and gradually assembled into filamentous structure. In the AL domain, a previous ingenious isotope labeling experiment confirmed that UTP binds before ATP. While the AL domain binds UTP and ATP, the GAT domain is also in the process of binding substrate GLN. After the combination of the two substrates, the start of AL domain reaction is recognized by the arch, and the tetramer gradually changes from open mode to closed mode.

In this process, GTP acts as a synchronizer, coordinating the reactions

catalyzed by the two domains and gradually improving the construction of ammonia channel. The β19 of the GAT domain, through the interaction between R481 and GTP, induces the closure of the GAT edge. At the same time, the reaction also makes CTPS continuously closed and the ammonia tunnel enters the closed state. With the upward movement of the wing and the effect of L4 in place of another protomer, the purine head of GTP is further stabilized.

Combined with the thioester intermediate previously simulated in the DON state, we believe that the wing, like a striker in a pistol, stimulates the tetrahedral intermediate in GAT to release ammonia, and goes to 4Pi-UTP in the AL domain along the constructed ammonia channel to complete the final reaction. After CTP synthesis, H55 and the arch retreated, the binding of GTP was no longer stable, and the tetramer also changed into an open state. The two domains released their products and waited for the next round of reaction.

In the whole reaction, GTP plays a crucial role in overall planning and coordination. Like the transmission device in the car, GTP synchronizes the consistent reaction steps of the two domains of the front and rear wheels and gradually stabilizes the ammonia channel. The wing, via the interaction with β19, serves as a striker in a pistol to trig the release of ammonia, which

is transmitted along the constructed ammonia channel to 4Pi-UTP, the target, completing the whole catalytic reaction.

At the same time, biochemical experiments also showed that the regulation of GTP on CTPS catalysis is sigmoid, indicating its fineness and robustness (Bearne et al., 2022; Bearne et al., 2001; Habrian et al., 2016; Kizaki et al., 1982; Lunn et al., 2008; MacDonnell et al., 2004; O'Sullivan et al., 1991; Simard et al., 2003; Willemoës, 2003; Willemoës et al., 2005). The establishment of GTP and ammonia channels has also served a checkpoint in the whole reaction. After DON inactivates the GAT domain, the establishment of intermediate tunnel fixes CTPS to avoid the continuous reaction of the AL domain (Zhou et al., 2021).

GTP is an important ligand for the function of G proteins and tubulins (Carlier, 1982; Hepler and Gilman, 1992). As a switch, GTP, is finally hydrolyzed into GDP. The hydrolysis of GTP is a very necessary part of many reactions. In our work, we find that GTP does not participate in the reaction, but acts as an enzymatic synchronizer. The relatively independent reactions catalyzed by the two domains of CTPS is synchronized by a small molecule GTP. GTP accomplishes the synchronization process through a series of checkpoints, which effectively improves the efficiency of enzyme reaction.

The new function suggests the importance of GTP as a multifunctional molecule. What is particularly expected is whether GTP acts as a synchronizer in the reaction of similar enzymes other than CTPS. A further immediate interesting question is: whether other small molecules also play the role of synchronizer like GTP in some multifunctional enzymes?

Methods

dmCTPS Expression and Purification

dmCTPS is expressed in Transetta (DE3), as described before.

Cryo-EM Grid Preparation and Data Collection

For the ACP state dmCTPS sample, dmCTPS protein was dissolved in the buffer with 25 mM Hepes, 2 mM UTP, 2 mM ACP, 2 mM GTP, and 10 mM MgCl2. For the MIX state dmCTPS sample, dmCTPS protein was dissolved in the buffer with 25 mM Hepes, 2 mM UTP, 2 mM ATP, 2 mM GTP, and 10 mM MgCl2. For both samples, 10mM Glutamine is used to start the reaction. Samples were prepared with amorphous alloy film (No. M024-Au300-R12/13) and FEI Vitrobot (8 °C temperature, 3.5 s blotting time, −5 blot force). Images were collected through Gatan K3 summit camera with 22,500X

magnification in super-resolution mode on a 300kv FEI Titan Krios electron microscope. For data collection, the defocus is set to 1.0-2.5 μm, pixel size is 1.06Å. The total dose was 60 e−/Å^2 subdivided into 50 frames at 4-s exposure using SerialEM.

Image Processing

Image processing flow is similar to that before, and was done in Relion3.1-beta. Raw images were corrected by MOTIONCOR2 through Relion3 GUI, contrast transfer function (CTF) parameters were determined by CTFFIND4. After 2D and 3D classifications, 209473, 353286 particles were used in 3D refinement for ACP and MIX state. To improve the resolution, CTF refinement and Bayesian polishing were applied. Finally, we constructed maps with resolution 3.3 Å for ACP state CTPS and 3.2 Å for MIX state CTPS.

3D variability analysis

3DVA was done in Cryosparc V3.3. After 3D refinement, particles with angle information were export from Relion to Cryosparc. To focus on a protomer of tetramer, symmetry collapse and a local mask were applied. 3D Variability was carried out with filter resolution 3.2Å and 3Å for ACP state and MIX state respectively. And results were displayed by a simple mode with 20 frames.

Model building and Refinement

Our previous models 7DPT and 7DPW were used as initial model. At first models of single chain were manually refined according to our electron density map with Coot software. Then D2 symmetry is used to generate other chains by Chimera software. Finally models for tetramer were real-space refined by Python-based hierarchical environment for integrated Xtallography (Phenix) software.

Tunnel Modeling

Model tunnels were calculated by CAVER Analyst software. Tunnel starting position is set to the active site of GAT domain and probe radii is set to 0.9Å during the calculation. ChimeraX software is used for result depiction.

Acknowledgments

We thank Jiale Zhong, Zherong Ryan Zhang, Zixuan Wang and Xiaojie Bao for technical support. EM data were collected at the ShanghaiTech Cryo-EM Imaging Facility. We thank the Molecular and Cell Biology Core Facility (MCBCF) at the School of Life Science and Technology, ShanghaiTech University for providing technical support. This work was supported by grants from Ministry of Science and Technology of China (No. 2021YFA0804701-4), National Natural Science Foundation of China (No. 31771490), and Shanghai Science and Technology Commission (No. 20JC1410500) for grants to J.L.L.

References

Anderson, P.M. (1983). CTP synthetase from *Escherichia coli*: an improved purification procedure and characterization of hysteretic and enzyme concentration effects on kinetic properties. Biochemistry *22*, 3285-3292.

Aronow, B., and Ullman, B. (1987). In situ regulation of mammalian CTP synthetase by allosteric inhibition. J Biol Chem *262*, 5106-5112.

Bakovic, M., Fullerton, M.D., and Michel, V. (2007). Metabolic and molecular aspects of ethanolamine phospholipid biosynthesis: the role of CTP:phosphoethanolamine cytidylyltransferase (Pcyt2). Biochem Cell Biol *85*, 283-300.

Bearne, S.L., Guo, C.-J., and Liu, J.-L. (2022). GTP-Dependent Regulation of CTP Synthase: Evolving Insights into Allosteric Activation and NH3 Translocation. Biomolecules *12*, 647.

Bearne, S.L., Hekmat, O., and MacDonnell, J.E. (2001). Inhibition of *Escherichia coli* CTP synthase by glutamate γ-semialdehyde and the role of the allosteric effector GTP in glutamine hydrolysis. Biochem J *356*, 223-232.

Cao, E., Liao, M., Cheng, Y., and Julius, D. (2013). TRPV1 structures in distinct conformations reveal activation mechanisms. Nature *504*, 113-118.

Carlier, M.F. (1982). Guanosine-5'-triphosphate hydrolysis and tubulin polymerization. Review article. Mol Cell Biochem *47*, 97-113.

Chakraborty, K.P., and Hurlbert, R.B. (1961). Role of glutamine in the biosynthesis of cytidine nucleotides in *Escherichia coli*. Biochim Biophys Acta *47*, 607-609.

Cheng, Y. (2015). Single-Particle Cryo-EM at Crystallographic Resolution. Cell *161*, 450-457.

Cheng, Y. (2018). Single-particle cryo-EM-How did it get here and where will it go. Science *361*, 876-880.

De Clercq, E. (1993). Antiviral agents: characteristic activity spectrum depending on the molecular target with which they interact. Adv Virus Res *42*, 1-55.

Endrizzi, J.A., Kim, H., Anderson, P.M., and Baldwin, E.P. (2004). Crystal structure of *Escherichia coli* cytidine triphosphate synthetase, a nucleotide-regulated glutamine amidotransferase/ATP-dependent amidoligase fusion protein and homologue of anticancer and antiparasitic drug targets. Biochemistry *43*, 6447-6463.

Endrizzi, J.A., Kim, H., Anderson, P.M., and Baldwin, E.P. (2005). Mechanisms of product feedback regulation and drug resistance in cytidine triphosphate synthetases from the structure of a CTP-inhibited complex. Biochemistry *44*, 13491-13499.

Goto, M., Omi, R., Nakagawa, N., Miyahara, I., and Hirotsu, K. (2004). Crystal structures of CTP synthetase reveal ATP, UTP, and glutamine binding sites. Structure *12*, 1413-1423.

Habrian, C., Chandrasekhara, A., Shahrvini, B., Hua, B., Lee, J., Jesinghaus, R., Barry, R., Gitai, Z., Kollman, J., and Baldwin, E.P. (2016). Inhibition of *Escherichia coli* CTP synthetase by NADH and other nicotinamides and their mutual interactions with CTP and GTP. Biochemistry *55*, 5554-5565.

Hepler, J.R., and Gilman, A.G. (1992). G proteins. Trends Biochem Sci *17*, 383-387.

Ingerson-Mahar, M., Briegel, A., Werner, J.N., Jensen, G.J., and Gitai, Z. (2010). The metabolic enzyme CTP synthase forms cytoskeletal filaments. Nat Cell Biol *12*, 739-746.

564 Iyengar, A., and Bearne, S.L. (2003). Aspartate 107 and leucine 109 facilitate efficient coupling of
565 glutamine hydrolysis to CTP synthesis by *E. coli* CTP synthase. Biochem J *369*, 497-507.
566 Jiménez, B.M., and O'Sullivan, W.J. (1994). CTP synthetase and enzymes of pyrimidine
567 ribonucleotide metabolism in *Giardia intestinalis*. Int J Parasitol *24*, 713-718.
568 Kizaki, H., Ohsaka, F., and Sakurada, T. (1982). Role of GTP in CTP synthetase from Ehrlich ascites
569 tumor cells. Biochem Biophys Res Commun *108*, 286-291.
570 Kizaki, H., Ohsaka, F., and Sakurada, T. (1985). CTP synthetase from Ehrlich ascites tumor cells.
571 Subunit stoichiometry and regulation of activity. Biochim Biophys Acta *829*, 34-43.
572 Kizaki, H., Sakurada, T., and Weber, G. (1981). Purification and properties of CTP synthetase from
573 Ehrlich ascites tumor cells. Biochim Biophys Acta *662*, 48-54.
574 Levitzki, A., and Koshland, D.E., Jr. (1969). Negative cooperativity in regulatory enzymes. Proc
575 Natl Acad Sci U S A *62*, 1121-1128.
576 Levitzki, A., and Koshland, D.E., Jr. (1971). Cytidine triphosphate synthetase. Covalent
577 intermediates and mechanisms of action. Biochemistry *10*, 3365-3371.
578 Levitzki, A., and Koshland, D.E., Jr. (1972a). Ligand-induced dimer-to-tetramer transformation in
579 cytosine triphosphate synthetase. Biochemistry *11*, 247-253.
580 Levitzki, A., and Koshland, D.E., Jr. (1972b). Role of an allosteric effector. Guanosine triphosphate
581 activation in cytosine triphosphate synthetase. Biochemistry *11*, 241-246.
582 Levitzki, A., Stallcup, W.B., and Koshland, D.E., Jr. (1971). Half-of-the-sites reactivity and the
583 conformational states of cytidine triphosphate synthetase. Biochemistry *10*, 3371-3378.
584 Lewis, D.A., and Villafranca, J.J. (1989). Investigation of the mechanism of CTP synthetase using
585 rapid quench and isotope partitioning methods. Biochemistry *28*, 8454-8459.
586 Liao, M., Cao, E., Julius, D., and Cheng, Y. (2013). Structure of the TRPV1 ion channel determined
587 by electron cryo-microscopy. Nature *504*, 107-112.
588 Liu, J.L. (2010). Intracellular compartmentation of CTP synthase in *Drosophila*. J Genet Genomics
589 *37*, 281-296.
590 Long, C.W., and Pardee, A.B. (1967). Cytidine triphosphate synthetase of *Escherichia coli* B. I.
591 Purification and kinetics. J Biol Chem *242*, 4715-4721.
592 Lunn, F.A., and Bearne, S.L. (2004). Alternative substrates for wild-type and L109A *E. coli* CTP
593 synthases. Kinetic evidence for a constricted ammonia tunnel. Eur J Biochem *271*, 4204-4212.
594 Lunn, F.A., MacDonnell, J.E., and Bearne, S.L. (2008). Structural requirements for the activation of
595 *Escherichia coli* CTP synthase by the allosteric effector GTP are stringent, but requirements for
596 inhibition are lax. J Biol Chem *283*, 2010-2020.
597 MacDonnell, J.E., Lunn, F.A., and Bearne, S.L. (2004). Inhibition of *E. coli* CTP synthase by the
598 "positive" allosteric effector GTP. Biochim Biophys Acta *1699*, 213-220.
599 McCluskey, G.D., and Bearne, S.L. (2018a). Biophysical analysis of bacterial CTP synthase
600 filaments formed in the presence of the chemotherapeutic metabolite gemcitabine-5'-
601 triphosphate. J Mol Biol *430*, 1201-1217.
602 McCluskey, G.D., and Bearne, S.L. (2018b). "Pinching" the ammonia tunnel of CTP synthase
603 unveils coordinated catalytic and allosteric-dependent control of ammonia passage. Biochim
604 Biophys Acta Gen Subj *1862*, 2714-2727.
605 McPartland, R.P., and Weinfeld, H. (1979). Cooperative effects of CTP on calf liver CTP
606 synthetase. J Biol Chem *254*, 11394-11398.
607 Noree, C., Sato, B.K., Broyer, R.M., and Wilhelm, J.E. (2010). Identification of novel filament-

608 forming proteins in *Saccharomyces cerevisiae* and *Drosophila melanogaster*. J Cell Biol *190*, 541-
609 551.
610 O'Sullivan, W.J., Jiminez, B.M., Dai, Y.P., and Lee, C.S. (1991). GTP activates two enzymes of
611 pyrimidine salvage from the human intestinal parasite *Giardia intestinalis*. Adv Exp Med Biol
612 *309B*, 249-452.
613 Ozier-Kalogeropoulos, O., Adeline, M.T., Yang, W.L., Carman, G.M., and Lacroute, F. (1994). Use
614 of synthetic lethal mutants to clone and characterize a novel CTP synthetase gene in
615 *Saccharomyces cerevisiae*. Mol Gen Genet *242*, 431-439.
616 Ozier-Kalogeropoulos, O., Fasiolo, F., Adeline, M.T., Collin, J., and Lacroute, F. (1991). Cloning,
617 sequencing and characterization of the *Saccharomyces cerevisiae* URA7 gene encoding CTP
618 synthetase. Mol Gen Genet *231*, 7-16.
619 Robertson, J.G., and Villafranca, J.J. (1993). Characterization of metal ion activation and inhibition
620 of CTP synthetase. Biochemistry *32*, 3769-3777.
621 Roy, A.C., Lunn, F.A., and Bearne, S.L. (2010). Inhibition of CTP synthase from *Escherichia coli* by
622 xanthines and uric acids. Bioorg Med Chem Lett *20*, 141-144.
623 Savage, C.R., and Weinfeld, H. (1970). Purification and properties of mammalian liver cytidine
624 triphosphate synthetase. J Biol Chem *245*, 2529-2535.
625 Simard, D., Hewitt, K.A., Lunn, F., Iyengar, A., and Bearne, S.L. (2003). Limited proteolysis of
626 *Escherichia coli* cytidine-5'-triphosphate synthase. Identification of residues required for CTP
627 formation and GTP-dependent activation of glutamine hydrolysis. Eur J Biochem *270*, 2195-
628 2206.
629 Steeves, C.H., and Bearne, S.L. (2011). Activation and inhibition of CTP synthase from
630 *Trypanosoma brucei*, the causative agent of African sleeping sickness. Bioorg Med Chem Lett *21*,
631 5188-5190.
632 Thomas, P.E., Lamb, B.J., and Chu, E.H. (1988). Purification of cytidine-triphosphate synthetase
633 from rat liver, and demonstration of monomer, dimer and tetramer. Biochim Biophys Acta *953*,
634 334-344.
635 van Kuilenburg, A.B., Elzinga, L., and van Gennip, A.H. (1998). Kinetic properties of CTP
636 synthetase from HL-60 cells. Adv Exp Med Biol *431*, 255-258.
637 van Kuilenburg, A.B., Meinsma, R., Vreken, P., Waterham, H.R., and van Gennip, A.H. (2000).
638 Isoforms of human CTP synthetase. Adv Exp Med Biol *486*, 257-261.
639 von der Saal, W., Anderson, P.M., and Villafranca, J.J. (1985). Mechanistic investigations of
640 *Escherichia coli* cytidine-5'-triphosphate synthetase. Detection of an intermediate by positional
641 isotope exchange experiments. J Biol Chem *260*, 14993-14997.
642 Weinfeld, H., Savage, C.R., and McPartland, R.P. (1978). CTP synthetase of bovine calf liver.
643 Methods Enzymol *51*, 84-90.
644 Weng, M.L., and Zalkin, H. (1987). Structural role for a conserved region in the CTP synthetase
645 glutamine amide transfer domain. J Bacteriol *169*, 3023-3028.
646 Willemoës, M. (2003). Thr-431 and Arg-433 are part of a conserved sequence motif of the
647 glutamine amidotransferase domain of CTP synthases and are involved in GTP activation of the
648 *Lactococcus lactis* enzyme. J Biol Chem *278*, 9407-9411.
649 Willemoës, M. (2004). Competition between ammonia derived from internal glutamine hydrolysis
650 and hydroxylamine present in the solution for incorporation into UTP as catalysed by
651 *Lactococcus lactis* CTP synthase. Arch Biochem Biophys *424*, 105-111.

Willemoës, M., Mølgaard, A., Johansson, E., and Martinussen, J. (2005). Lid L11 of the glutamine amidotransferase domain of CTP synthase mediates allosteric GTP activation of glutaminase activity. FEBS J *272*, 856-864.

Willemoës, M., and Sigurskjold, B.W. (2002). Steady-state kinetics of the glutaminase reaction of CTP synthase from *Lactococcus lactis*. Eur J Biochem *269*, 4772-4779.

Williams, J.C., Kizaki, H., Weber, G., and Morris, H.P. (1978). Increased CTP synthetase activity in cancer cells. Nature *271*, 71-73.

Wu, Z., and Liu, J.L. (2022). CTP synthase does not form cytoophidia in Drosophila interfollicular stalks. Exp Cell Res, 113250.

Yang, W.L., Bruno, M.E., and Carman, G.M. (1996). Regulation of yeast CTP synthetase activity by protein kinase C. J Biol Chem *271*, 11113-11119.

Yang, W.L., and Carman, G.M. (1995). Phosphorylation of CTP synthetase from *Saccharomyces cerevisiae* by protein kinase C. J Biol Chem *270*, 14983-14988.

Zhou, X., Guo, C.J., Chang, C.C., Zhong, J., Hu, H.H., Lu, G.M., and Liu, J.L. (2021). Structural basis for ligand binding modes of CTP synthase. Proc Natl Acad Sci USA *118*, e2026621118.

Figure legends

Figure 1. Overall structures dmCTPS tetramer in ACP state.

A) Cryo-EM reconstruction of CTPS tetramer in ACP state. Protomers are colored differently. Positions of adjacent tetramers within filament are indicated by the soft mask.

B) CTPS filament interface models. Relative amino acids of each protomers are displayed in different styles.

C) The CTPS monomer model shows the binding sites of ligands. They are colored in orchid, misty blue and orange, respectively.

D-E) Zoom in for ACP and UTP binding pocket. Map density is displayed by mesh.

F) Zoom in for GAT pocket. The density shows the interaction between catalytic triad and the substrate GLN.

Figure 2.The motion of CTPS in ACP state reveals that GTP stimulates GAT reaction.

A) B factors are shown for ACP state model.

B) Motion of GAT domain. The open and closed states are colored in magenta and purple respectively.

C) Display of 3D variability results and compare with DON state. The

model of DON state is colored in dodger blue. Red and blue dashed boxes represent GAT pocket and GTP binding sites, respectively.

Figure 3. Capture of GTP binding in reaction state.

A) Cryo EM reconstruction for MIX state CTPS tetramer. Protomers are colored differently. Positions of adjacent tetramers within filament were indicated by the soft mask.

B) CTPS filament interface models. Relative amino acids of each protomers are displayed in different styles.

C -F) Ligand binding sites for GLN, UTP, ATP and GTP, respectively.

G) Compared with the DON state of GTP binding site, it indicates that R481 and wing play a role in GTP recognition and combination. DON state model is colored in sky blue and its GTP is colored in grey. The wing is colored in lavender and orange arrows indicating DON and MIX state. The interaction between R481 and GTP is indicated by lavender and orange dashes as DON and MIX state.

H) Compared with the ACP state of GTP binding site, it shows that R481 plays a role in GTP recognition and combination. ACP state model is colored in purple.

Figure 4. Conformational changes show the arch coordinates with GTP to couple the two reactions of GAT and AL domains of CTPS.

A) The motion of GAT domain in CTPS reaction. Models from open to closed state (frame 0, 5, 10, 14, 19) are colored with Salmon, Moccasin, Light Cyan, Light Sky Blue, and Lavender respectively.

B) At frame 0, the first step reaction of AL domain has not yet occurred, GAT domain does not bind ligands, and GTP does not form a stable binding with CTPS.

C) The motion of CTPS from frame 0 to frame 5. CTPS shows a closed trend as a whole, and the GAT domain is close to AL domain.

D) With the movement of UTP, the arch begins to move to the AL domain and the whole AL domain begins to close. The GAT domain is also combining substrates and moving closer to the AL domain.

E) The motion of CTPS from frame 6 to frame 10. CTPS continues to close and the GAT domain continues to move to the AL domain.

F) The binding of GTP depends on the progress of AL domain and GAT domain reactions. Arch plays a key role in identifying and coordinating the interaction with GTP.

Figure 5. Conformational changes show that the coordination among R481, wing and GTP couples the two reactions of GAT and AL domains of CTPS.

A) The motion of CTPS from frame 10 to frame 14. After GTP binding, CTPS continues to change to the closed state, and the reaction in the two domains continues.

B) In frame 14, the interaction of H55 and UTP becomes stronger, which makes the arch move to AL domain. The movement of the arch also prompts GTP to combine with it to approach the AL domain. R481 enhances the interaction between GAT domainand GTP.

C) The motion of CTPS from frame 14 to frame 19. The stable binding of GTP drives CTPS into closed state.

D) The interaction between R481 and GTP paves the way for the interaction between wing and GTP.

Figure 6. GTP controls the formation of transient ammonia tunnel.

A) Tunnel and the leakage pore of ACP state. Map density is represented by a surface. The centerline of the tunnel is represented in the sphere style and colored in dodger blue and grey.

B) Graph of diameter of ammonia tunnel along its length in ACP state dmCTPS.

C) Zoom in for the leakage pore. The simulated surface for ACP state model is colored by white and transparent.

D) Zoom in for the exit of ammonia tunnel at AL domain with map density displayed.

E) Tunnel and two likely leakage pores of MIX state. Map density is represented by a surface. The centerline of the tunnel is represented in the sphere style and colored in dodger blue, grey and yellow.

F) Graph of diameter of ammonia tunnel along its length in MIX state dmCTPS.

G) Zoom in for the leakage pores. With the combination of GTP, the leakage pore of the ammonia tunnel is limited.

H) Zoom in for the exit of ammonia tunnel at AL domain.

Figure 7. Model for GTP synchronizing CTPS reaction.

Without GTP, the reactions of AL and GAT are independent of each other and will not form the ammonia tunnel. Ammonia diffuses freely between the two domains. When GTP is present, GTP recognizes and synchronizes the reaction of GAT and AL through the interaction with L11 and the arch. R481 strengthens the binding with GTP and initiates its coupling with GTP. Under the synchronization and multiple interactions with AL and GAT domains of GTP, CTPS gradually closes and further wraps GTP between the two domains. Meanwhile, the preliminary construction of ammonia channel has been completed. Finally, with the compaction of L4 and the wing, GTP stimulates the release of ammonia to complete the synthesis of CTP. After CTP synthesis, the arch retreated, the binding of GTP was no longer stable, and the tetramer became open.

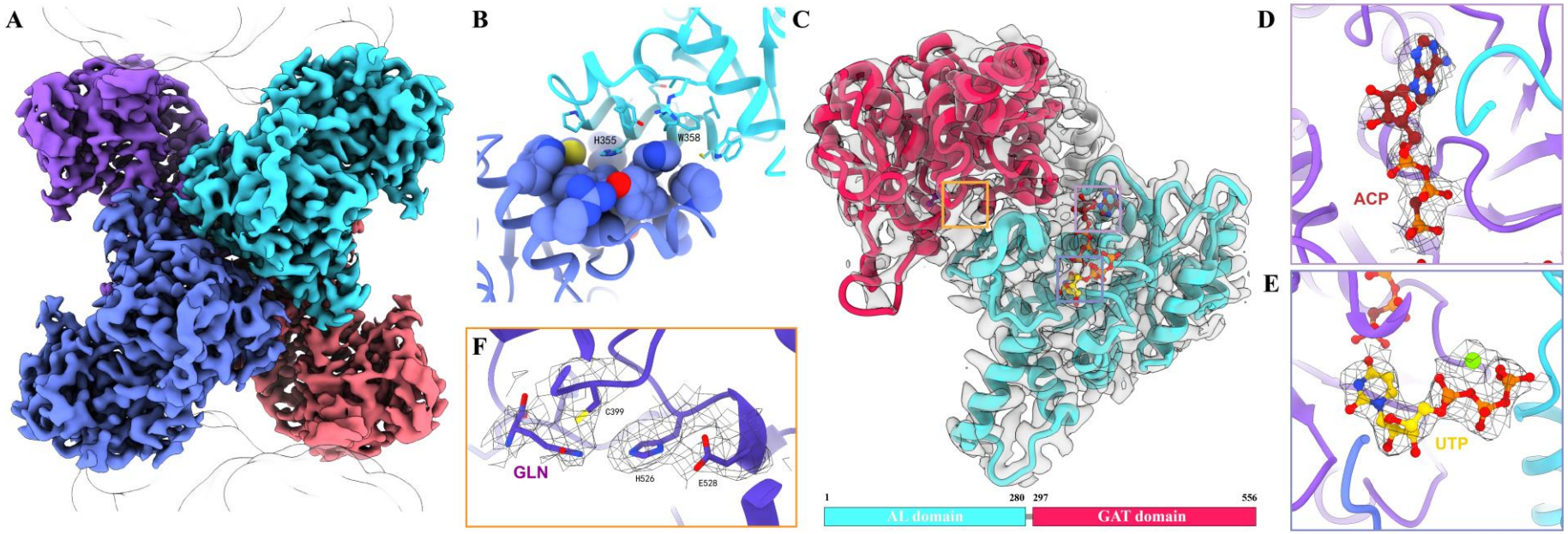
A
B
H355
W358
C
D
ACP
E
UTP
F
C399
GLN
H526
E528
1
280
297
556
AL domain
GAT domain

Figure 1

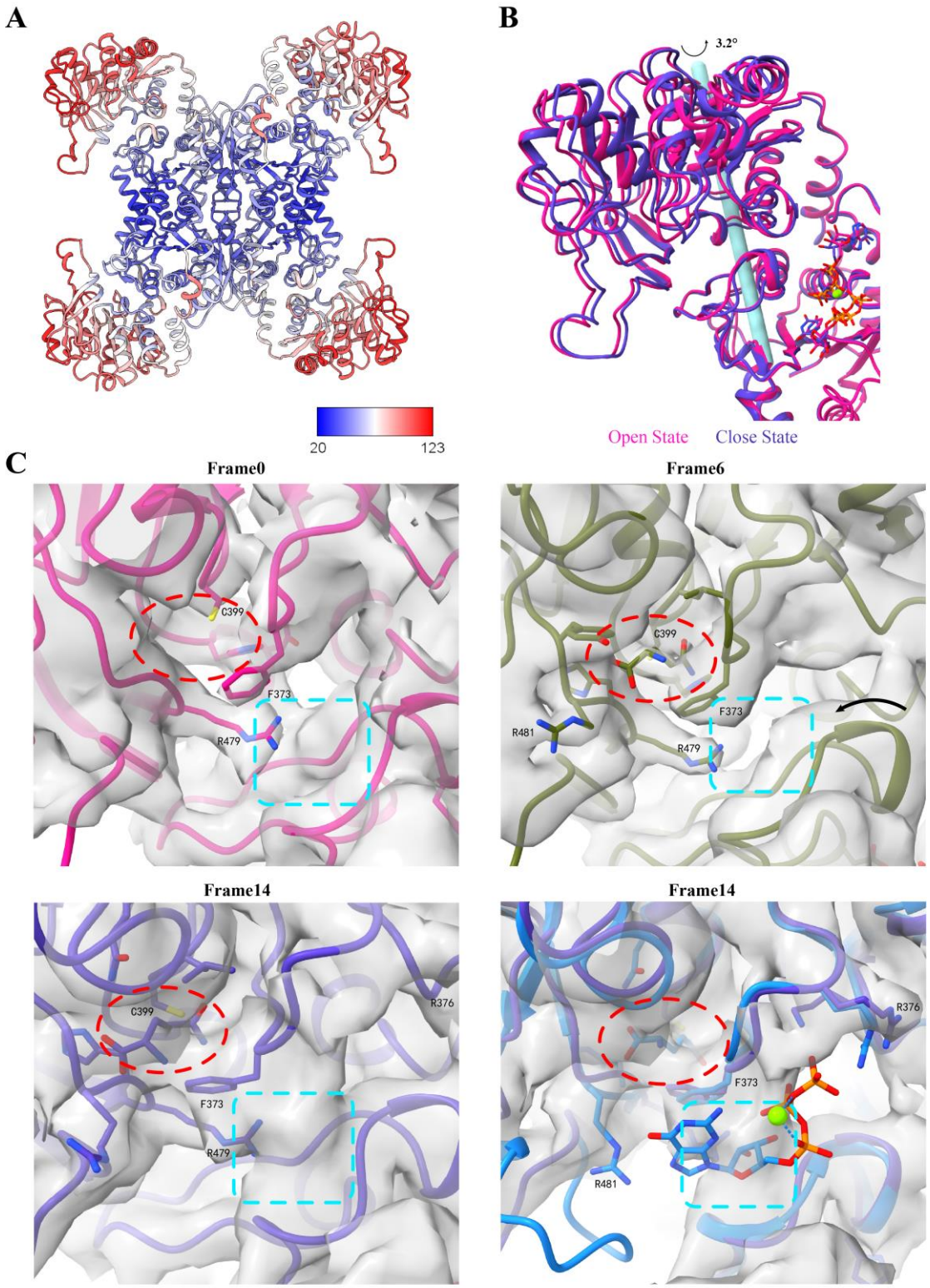

792

793 **Figure 2**

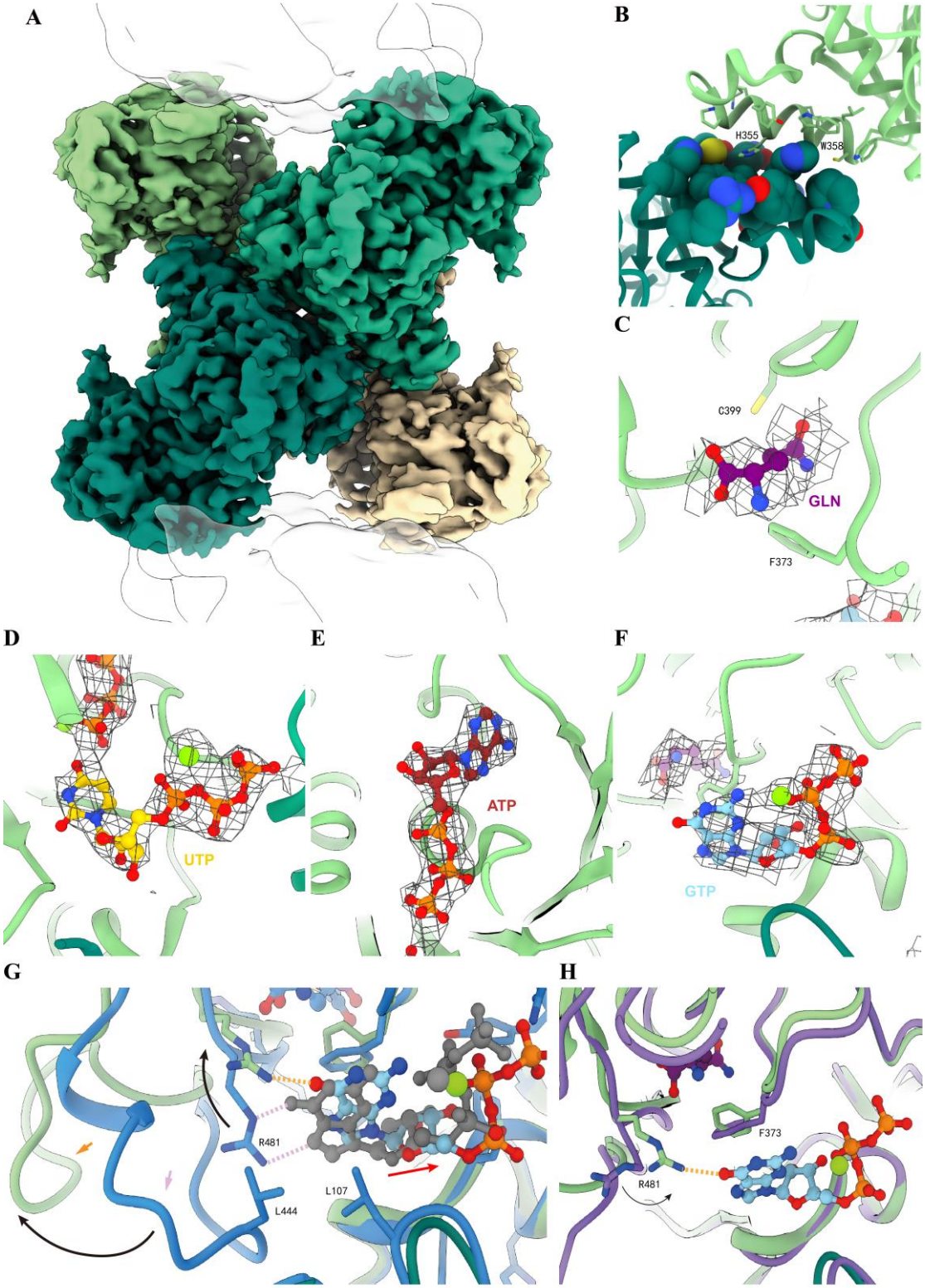
A
B
H355
W358
C
C399
GLN
F373
D
UTP
E
ATP
F
GTP
G
R481
L444
L107
H
F373
R481

Figure 3

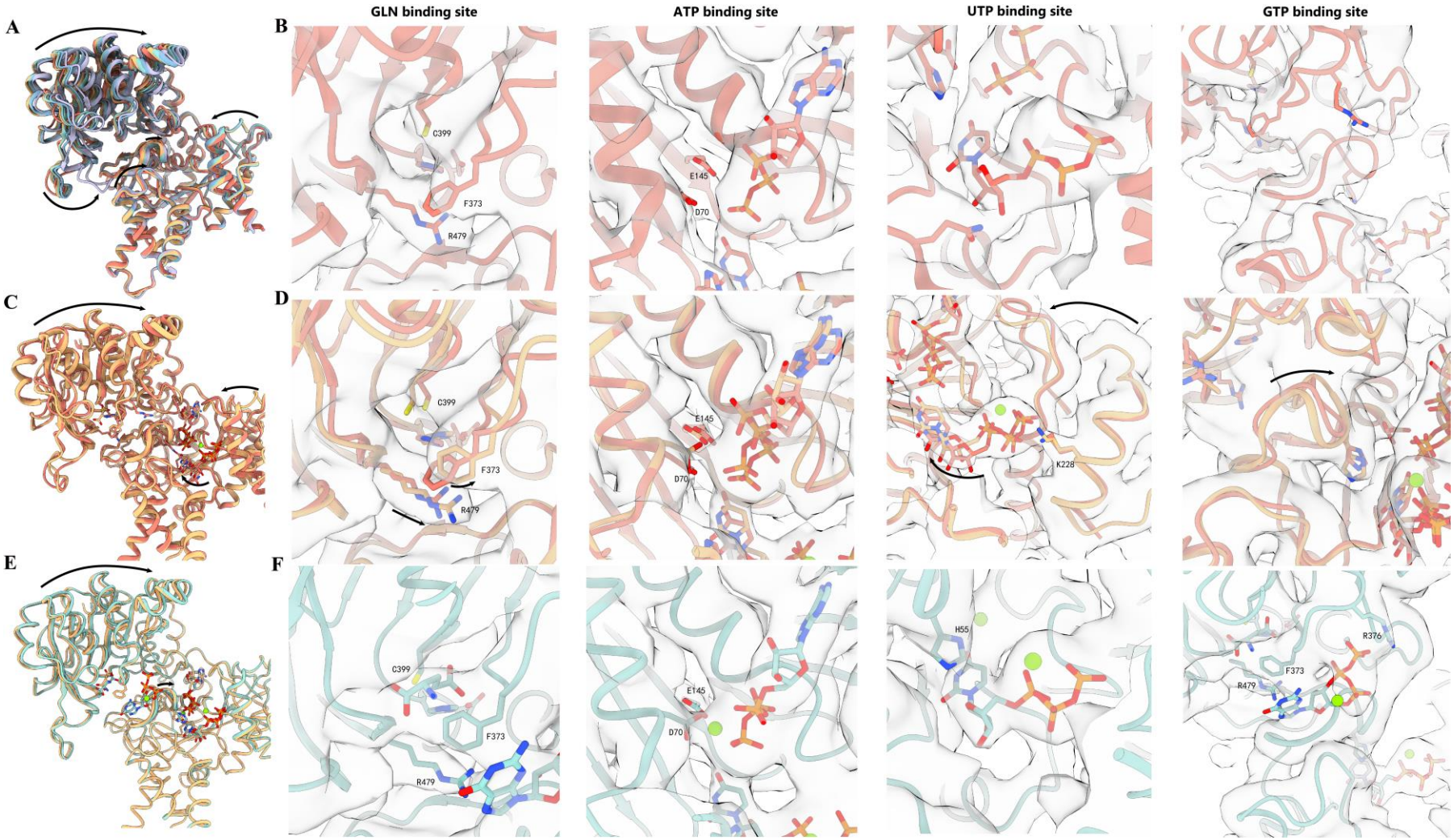
A
B
GLN binding site
ATP binding site
UTP binding site
GTP binding site
C399
F373
R479
E145
D70
C
D
K228
E
F
H55
R376

Figure 4

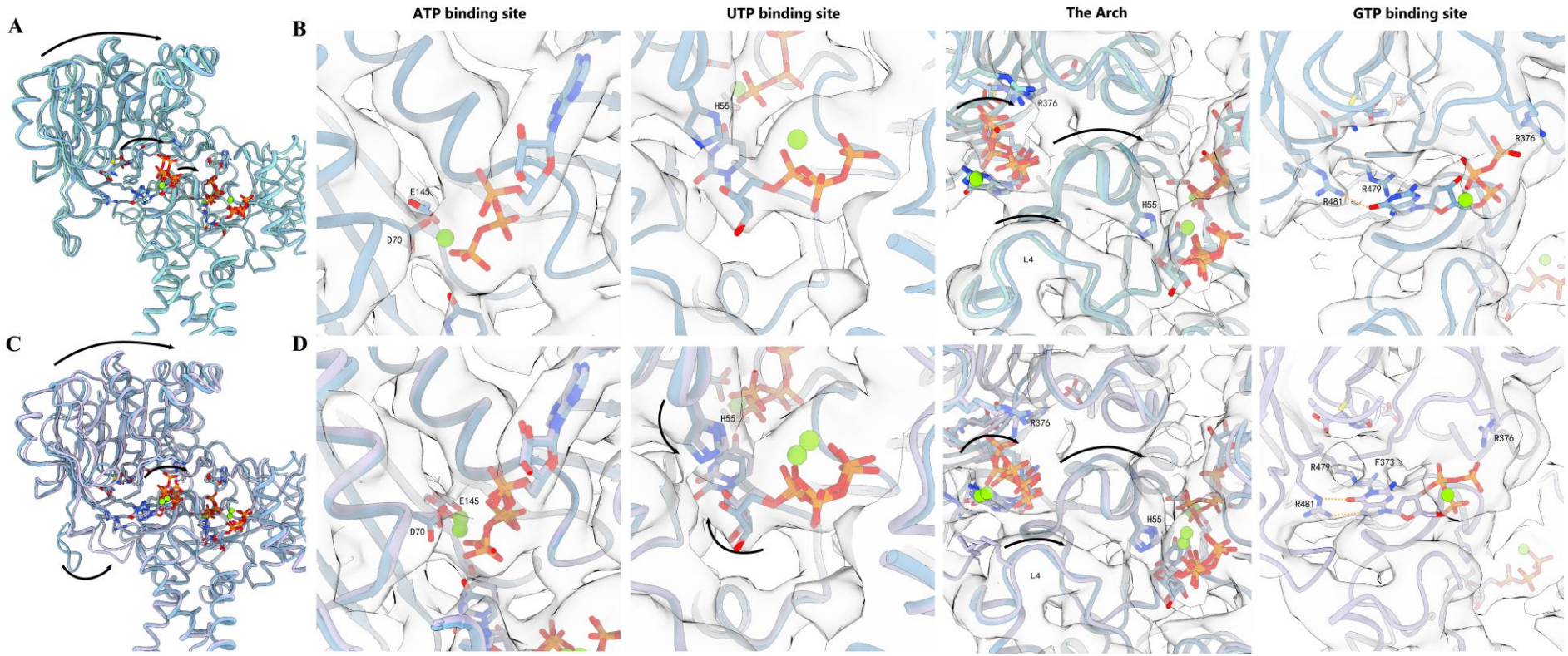
A
B
ATP binding site
UTP binding site
The Arch
GTP binding site
E145
D70
H55
R376
H55
L4
R376
R479
R481
C
D
E145
D70
H55
R376
H55
L4
R376
R479
F373
R481

Figure 5

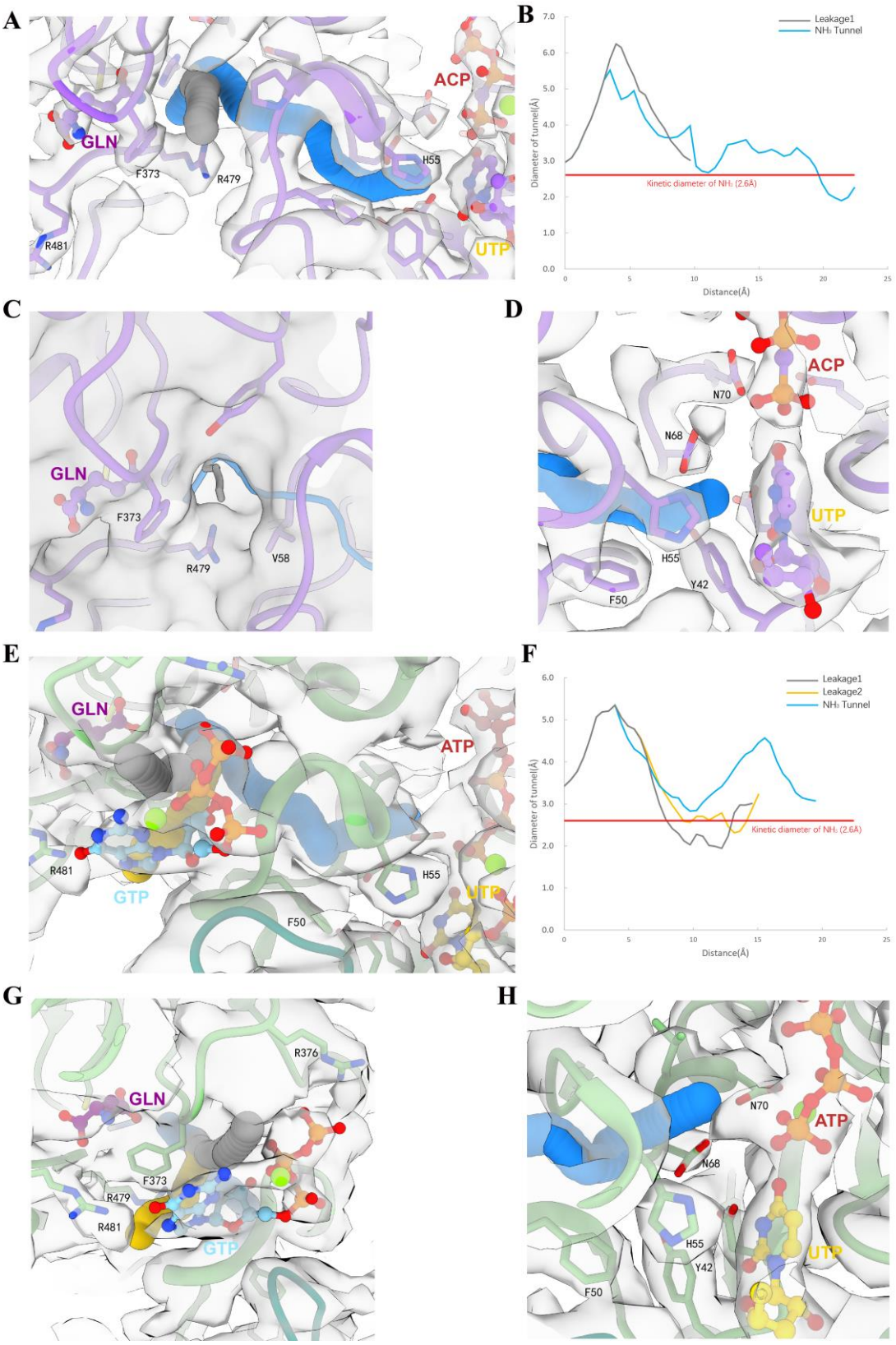
A
ACP
GLN
F373
R479
H55
R481
UTP
B
Leakage1
NH₃ Tunnel
Diameter of tunnel(Å)
Kinetic diameter of NH₃ (2.6Å)
Distance(Å)
C
GLN
F373
R479
V58
D
ACP
N70
N68
UTP
H55
Y42
F50
E
GLN
ATP
R481
GTP
H55
UTP
F50
F
Leakage1
Leakage2
NH₃ Tunnel
Diameter of tunnel(Å)
Kinetic diameter of NH₃ (2.6Å)
Distance(Å)
G
R376
GLN
F373
R479
R481
GTP
H
N70
ATP
N68
H55
Y42
UTP
F50

Figure 6

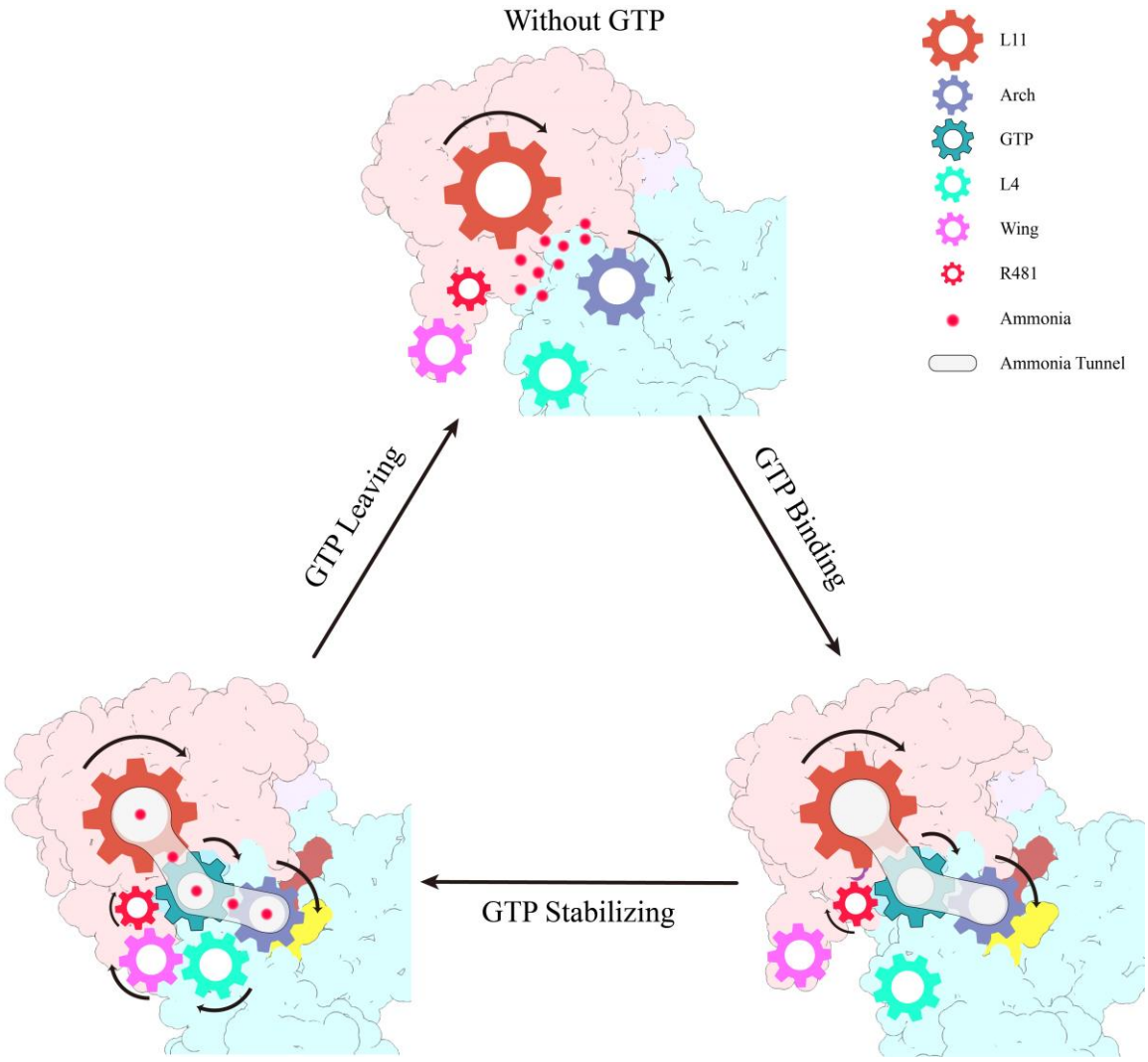
Without GTP
L11
Arch
GTP
L4
Wing
R481
Ammonia
Ammonia Tunnel
GTP Binding
GTP Stabilizing
GTP Leaving

Figure 7

Supplemental information

Supplemental figure legends

Figure S1. Catalysis and inhibition mechanism of CTPS.

C) The GAT and AL domains are represented by red and light blue boxes respectively. The GAT domain catalyzes the hydrolysis of GLN to generate ammonia. Ammonia is transferred to the AL domain through the ammonia tunnel. In the AL domain, the substrate UTP is phosphorylated by ATP to generate the intermediate 4Pi-UTP. Then 4Pi-UTP is converted to CTP in the presence of ammonia. GTP is an important allosteric regulator of CTPS.

D) DON is an analog of the substrate GLN. It can form covalent bonds with the catalytic cysteine of the GAT domain, thereby irreversibly inhibiting CTPS.

E) ACP is an analog of the substrate ATP. It can reversibly inhibit CTPS by completing with substrate ATP.

Figure S2. Image processing workflow of ACP state dmCTPS tetramer.

In the reconstruction of the ACP state dmCTPS tetramer, we collect 3669 micrographs and 209473 particles are kept after 3D classification. After re-extraction of particles of ACP state tetramer, different reconstructions are performed to generate the final map and model.

Figure S3. Statistics of the final density maps of the ACP state CTPS.

A) Representative cryo-EM micrograph of ACP state CTPS.

B) Representative 2D class averages of different views of the ACP state tetramer.

C) In the last iteration of the 3D auto-refinement, particle orientation distributions of the ACP state tetramer

D) Local resolution map of the ACP state tetramer final 3D density map.

E) Gold-standard FSC curve of the final density maps of the ACP state tetramer.

Figure S4. Conformational comparation of CTPS in DON, CTP, ACP states.

A) Conformational changes of GAT domain in DON, CTP and ACP

states. They are colored in dodger blue, orange and orchid respectively.

B) The ligand binding mode of ACP state differs from that of DON state. The model in DON state is colored by lime and transparent.

C) Separation of ACP and UTP densities indicates success inhibition by ACP.

Figure S5. Image processing workflow of MIX state dmCTPS tetramer.

In the reconstruction of the ACP state tetramer, we collect 3365 micrographs and retained 437045 particles after 3D classification. After re-extraction of particles of ACP state tetramer, different reconstructions are performed to generate the final map and model.

Figure S6. Statistics of final density maps of CTPS in MIX state.

A) Representative cryo-EM micrograph of MIX state CTPS.

B) Representative 2D class averages of different views of the MIX state tetramer.

C) Particle orientation distributions of the MIX state tetramer in the last iteration of the 3D auto-refinement.

D) Local resolution map of final 3D density map of the MIX state

tetramer.

E) Gold standard FSC curve of final density maps of the MIX state tetramer.

Figure S7. Conformational comparison of CTPS in DON, CTP, ACP and MIX states.

A) The ligand binding mode of the MIX state is similar to that of the ACP state. The model of ACP state is colored in purple and transparent.

B) Conformational comparison of DON, CTP and MIX states suggest that CTPS is not completely closed. Models for each state are colored in dodger blue, orange and green respectively.

Figure S8. Restriction residue graph of the ammonia tunnel in ACP and MIX states.

The upper panel shows the diameter of ammonia tunnel along its length from GAT pocket to AL pocket. The lower panel shows the restriction residues at each position, and their hydrophobicity is represented by color. A) The ACP state. B) The MIX state.

Figure S9. Through the interaction with L4 and the wing, GTP further stabilizes the ammonia tunnel.

I) Tunnel and the leakage pore of DON state. Map density is represented by a surface. The centerline of the tunnel is represented in the sphere style and colored in dodger blue and grey.

J) Diameter graph of ammonia tunnel along its length in DON state dmCTPS.

K) Zoom in for the leakage pore. L4 and the wing are embedded in GTP to make ammonia tunnel more stable.

L) Zoom in for the exit of ammonia tunnel at AL domain to display the map density. The exit of ammonia tunnel is close to 4Pi-UTP, which is beneficial to the next reaction.

Supplemental movie

Movie S1

3D variance analysis of the GAT domain reveals the transient interaction of GTP with CTPS during GAT reaction.

The movie displays the appearance of GTP during the GAT reaction. A molecular model of GTP is used as a marker for display.

Movie S2

3D variance analysis of CTPS reveals the synchronization effect of GTP for CTPS reaction.

The movie displays the conformational changes of CTPS from open state without GTP binding to closed state with GTP binding. A molecular model of GTP is used as a marker for display.

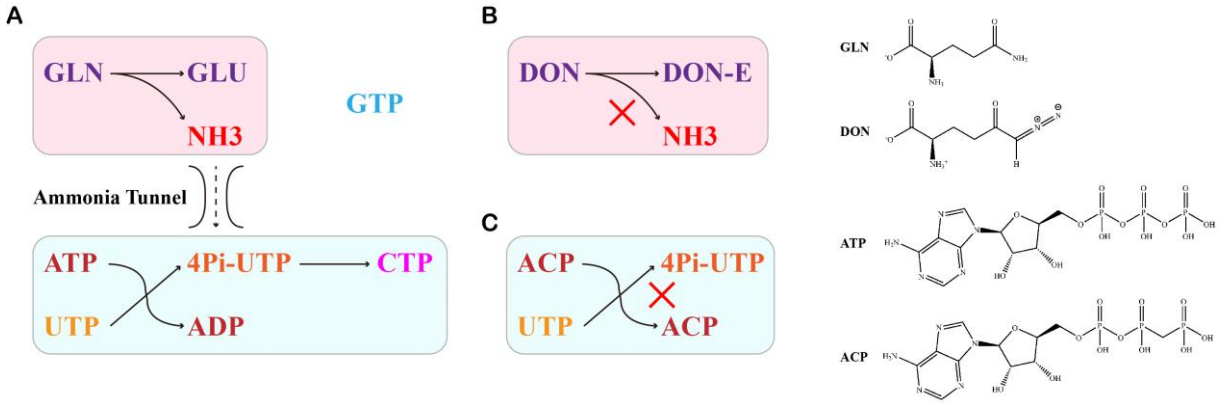

Supplementary Figure S1

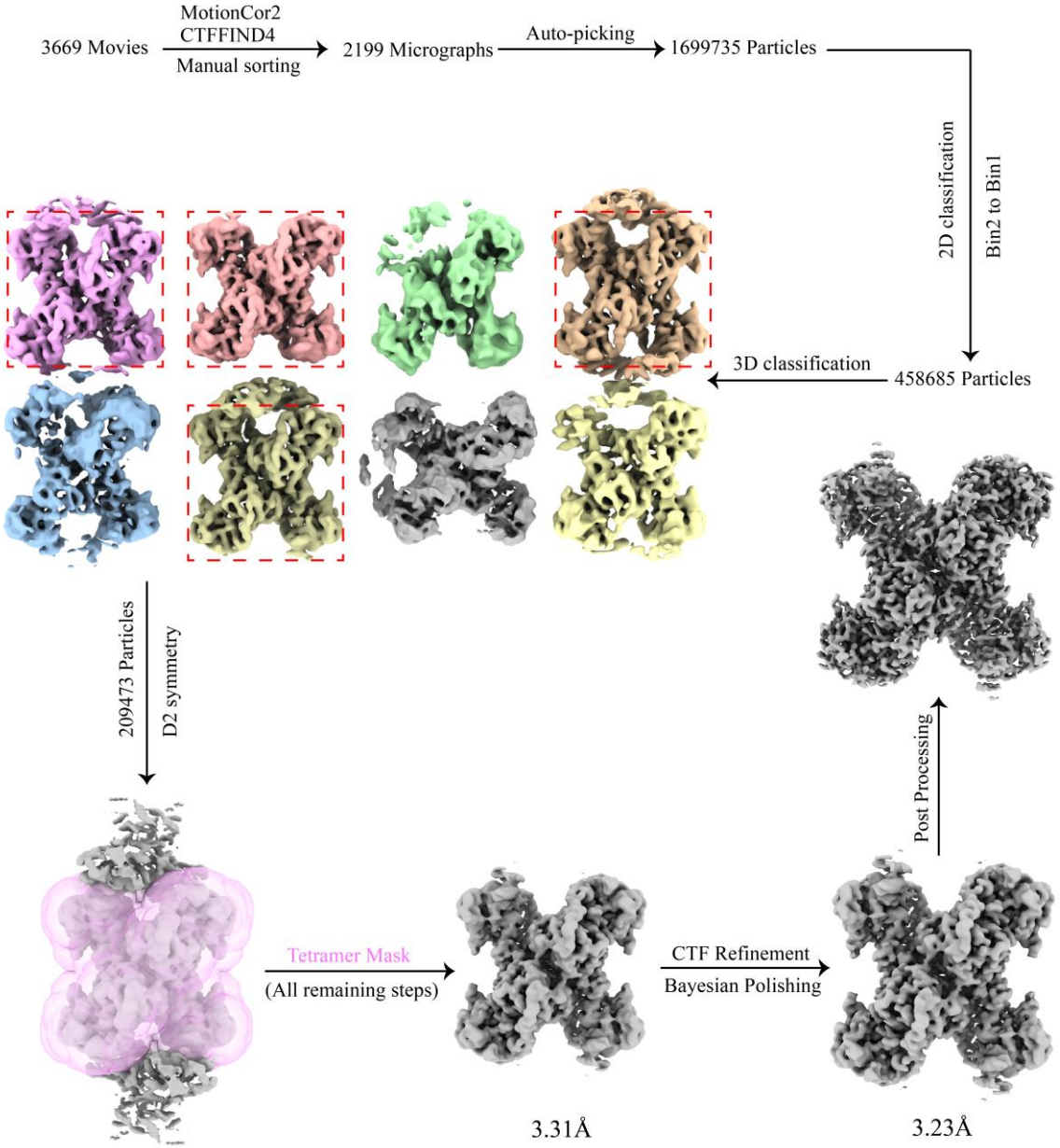

Supplementary Figure S2

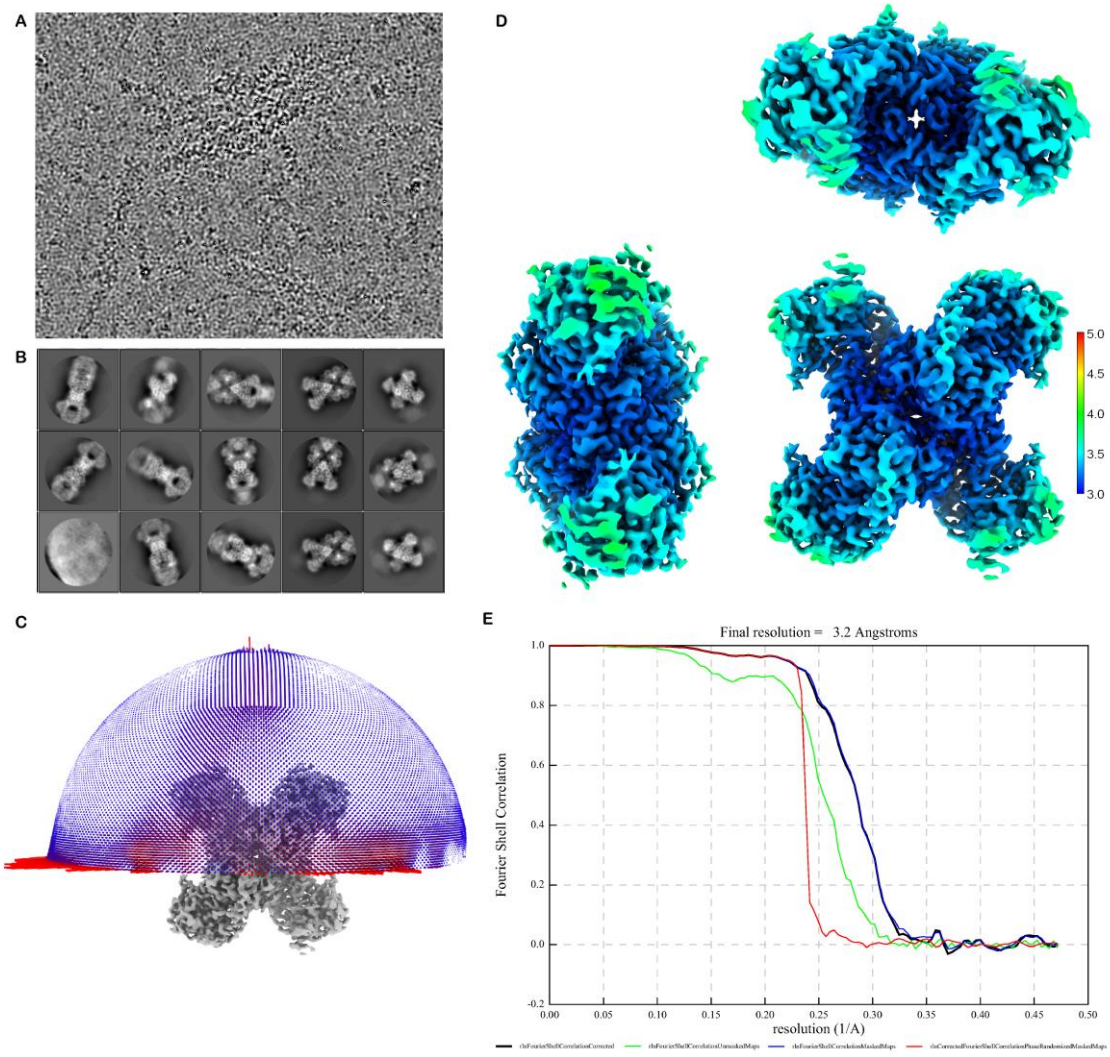

Supplementary Figure S3

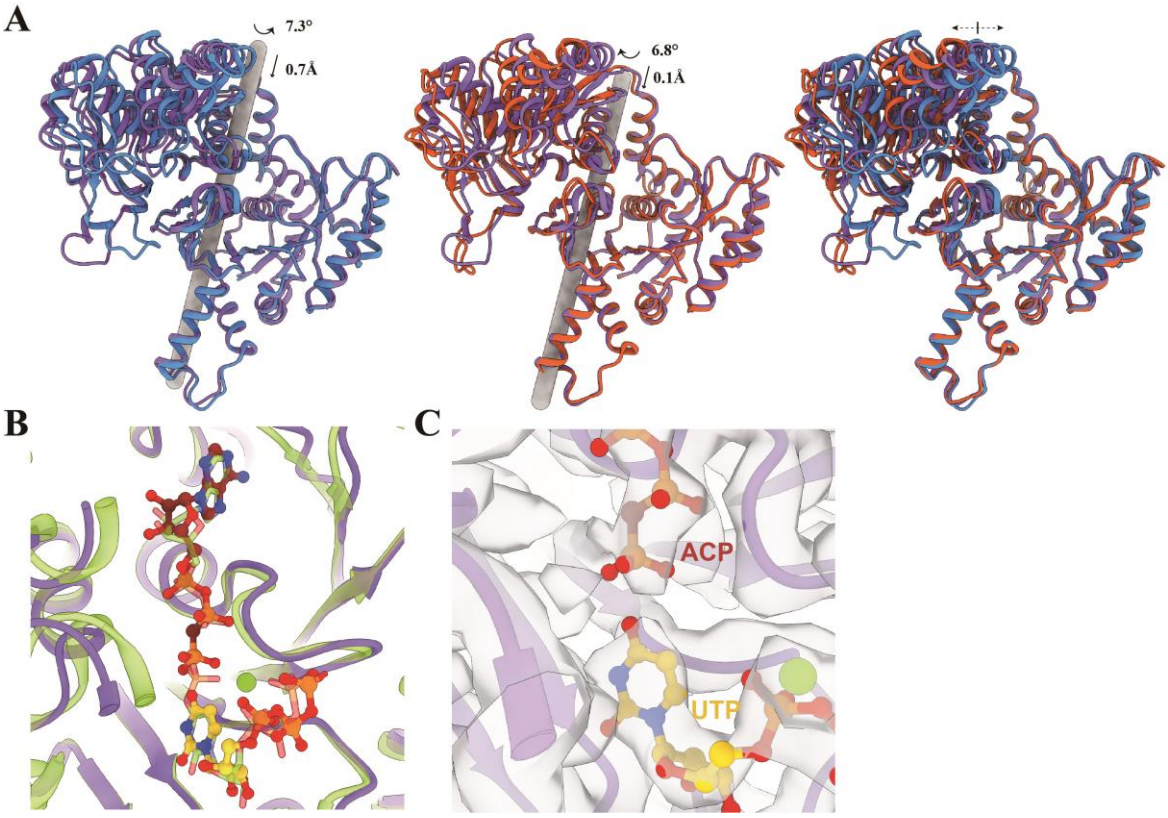

Supplementary Figure S4

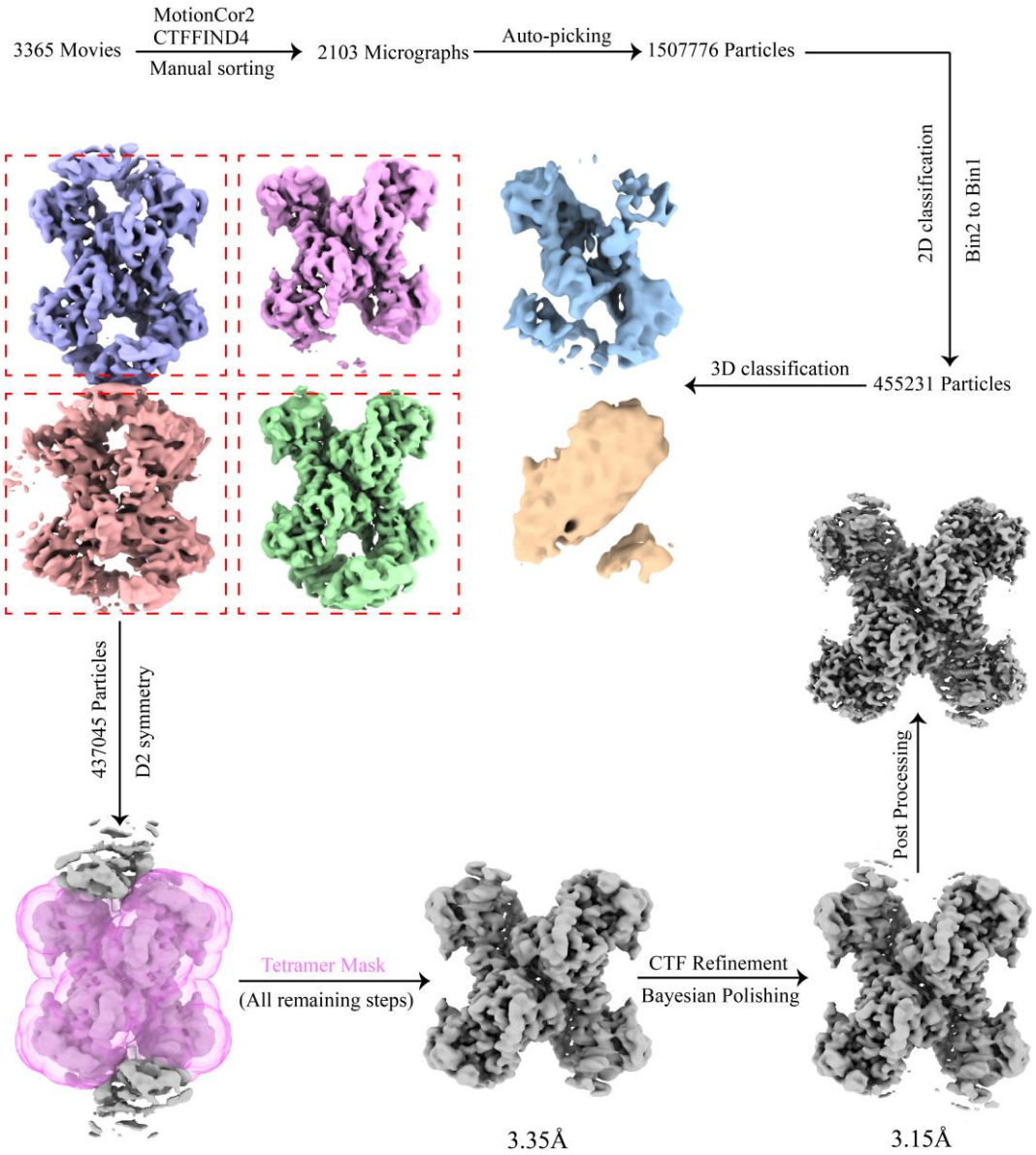

Supplementary Figure S5

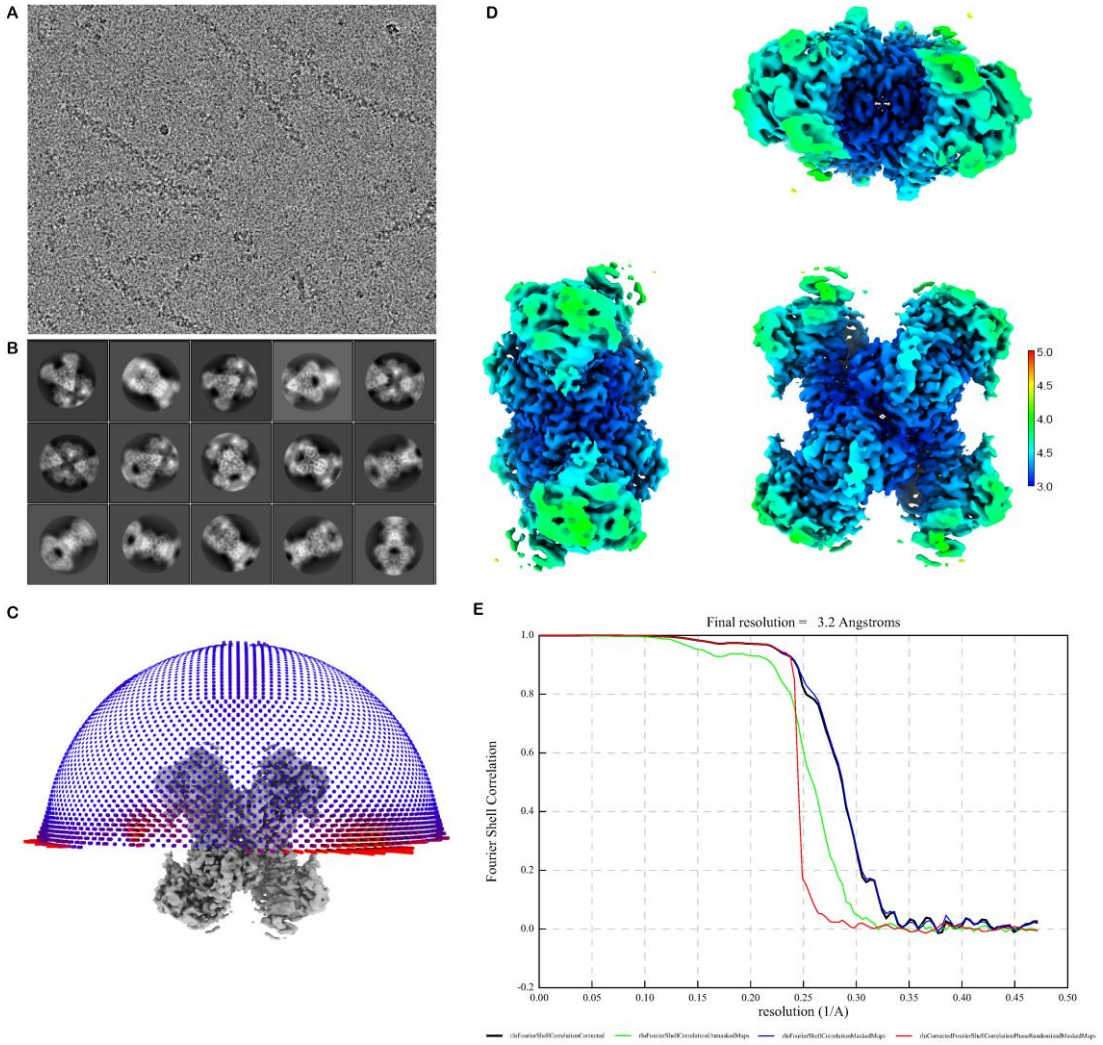

933

934 **Supplementary Figure S6**

935

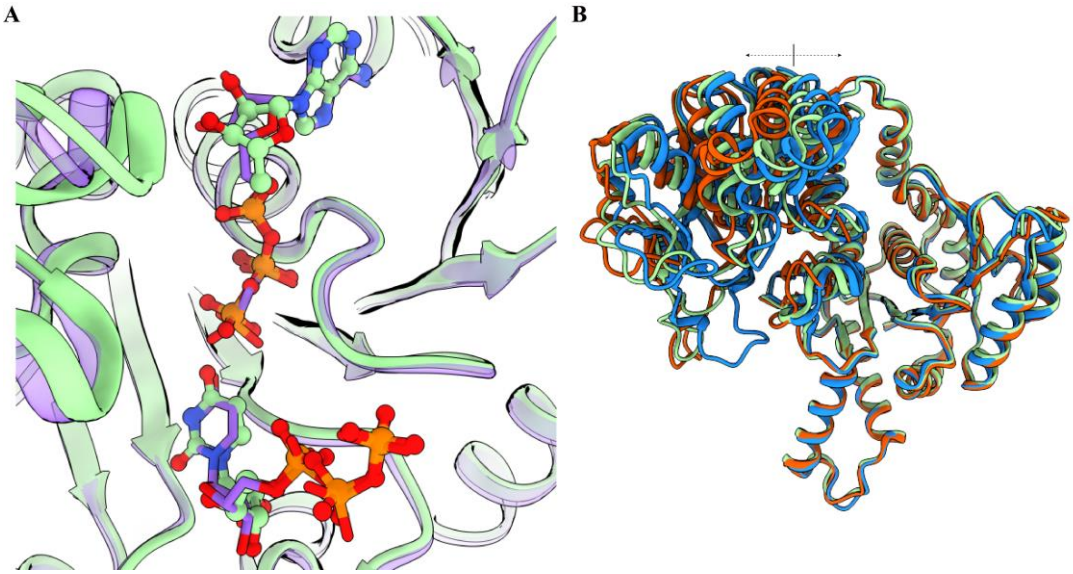

Supplementary Figure S7

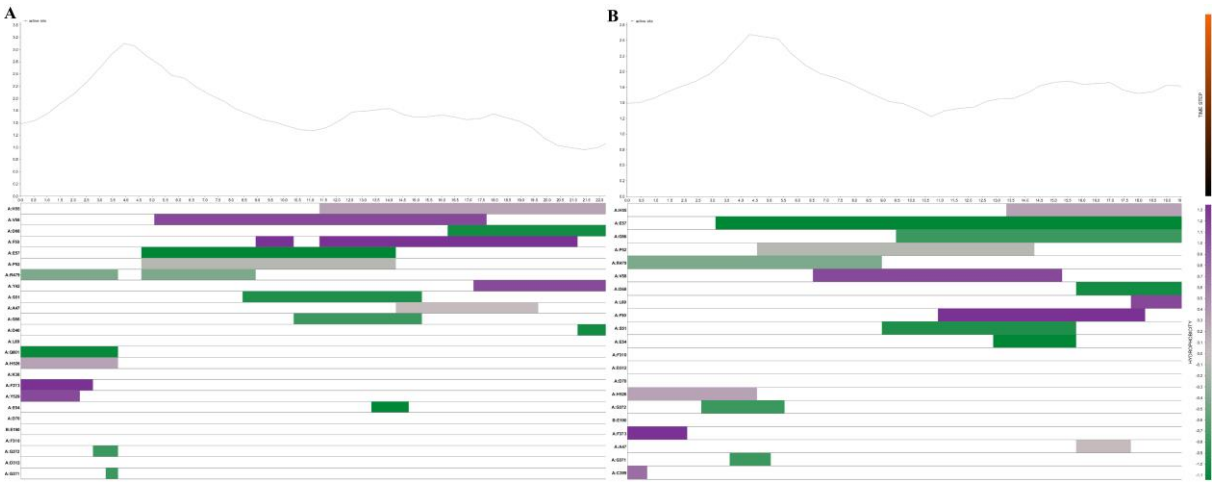

Supplementary Figure S8

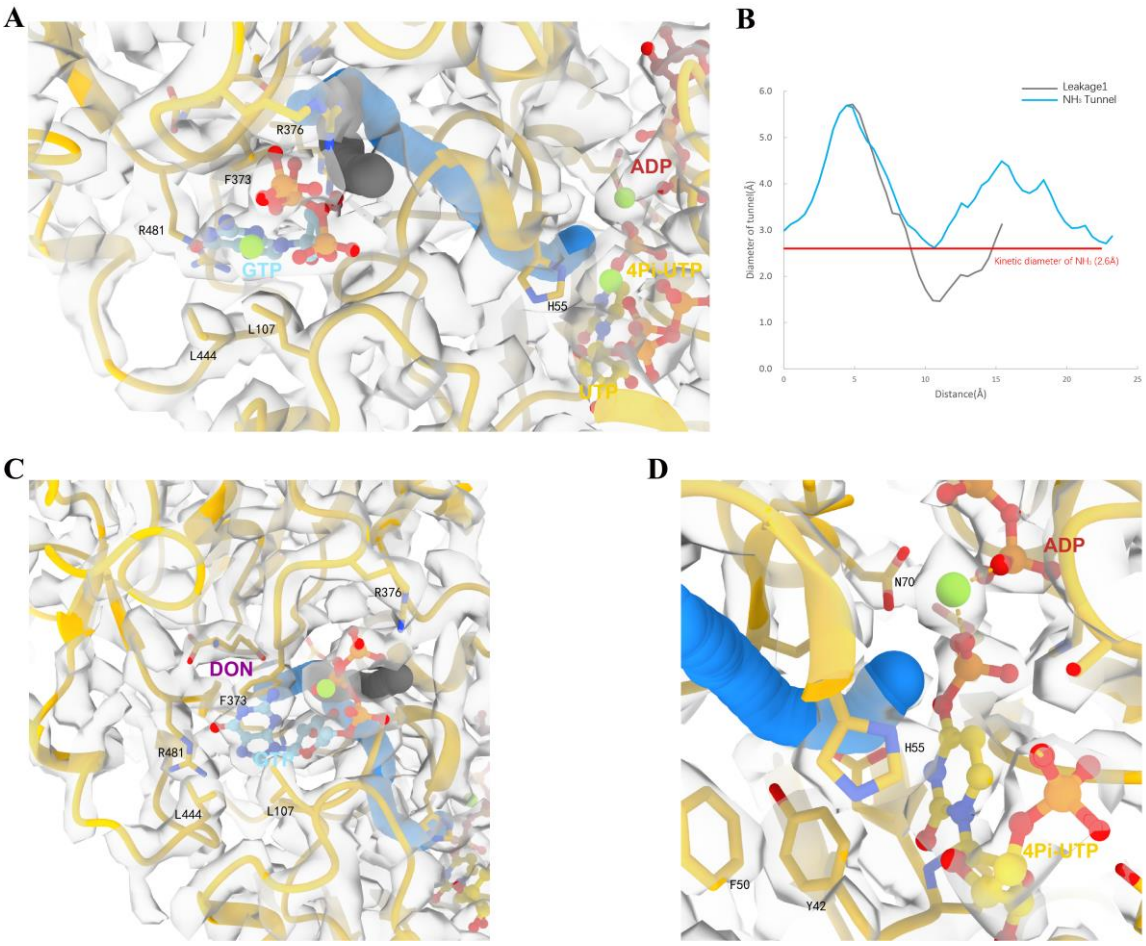

Supplementary Figure S9